BIOCHEMISTRY
including biophysical chemistry & molecular biology
Article

Biochemistry **2010,** *49,* 10595–10605 10595
DOI: 10.1021/bi101394r

Limiting an Antimicrobial Peptide to the Lipid−Water Interface Enhances Its Bacterial Membrane Selectivity: A Case Study of MSI-367[†]

Sathiah Thennarasu,[‡,§,⊥] Rui Huang,[§] Dong-Kuk Lee,[‡,§,⊗] Pei Yang,[‡] Lee Maloy,[∥] Zhan Chen,[‡,§] and Ayyalusamy Ramamoorthy*[,‡,§]

[‡]*Department of Biophysics, and* [§]*Department of Chemistry, University of Michigan, Ann Arbor, Michigan 48109-1055, United States,* [∥]*Genaera Pharmaceuticals, Plymouth Meeting, Pennsylvania 19462, United States.* [⊥]*Present address: Organic Chemistry Laboratory, Central Leather Research Institute, Adayaru, Chennai 600 020, India, and* [⊗]*Present address: Department of Fine Chemistry, Seoul National University of Technology, Seoul, Korea 139-743.*

Received August 29, 2010; Revised Manuscript Received November 9, 2010

ABSTRACT: In a minimalist design approach, a synthetic peptide MSI-367 [$(KFAKKFA)_3$-NH_2] was designed and synthesized with the objective of generating cell-selective nonlytic peptides, which have a significant bearing on cell targeting. The peptide exhibited potent activity against both bacteria and fungi, but no toxicity to human cells at micromolar concentrations. Bacterial versus human cell membrane selectivity of the peptide was determined via membrane permeabilization assays. Circular dichroism investigations revealed the intrinsic helix propensity of the peptide, β-turn structure in aqueous buffer and extended and turn conformations upon binding to lipid vesicles. Differential scanning calorimetry experiments with 1,2-dipalmitoleoyl-*sn*-glycero-3-phosphatidylethanolamine bilayers indicated the induction of positive curvature strain and repression of the fluid lamellar to inverted hexagonal phase transition by MSI-367. Results of isothermal titration calorimetry (ITC) experiments suggested the possibility of formation of specific lipid−peptide complexes leading to aggregation. ^{2}H nuclear magnetic resonance (NMR) of deuterated 1-palmitoyl-2-oleoyl-*sn*-glycero-3-phosphatidylcholine (POPC) multilamellar vesicles confirmed the limited effect of the membrane-embedded peptide at the lipid−water interface. ^{31}P NMR data indicated changes in the lipid headgroup orientation of POPC, 1-palmitoyl-2-oleoyl-*sn*-glycero-3-phosphatidylglycerol, and 1-palmitoyl-2-oleoyl-*sn*-glycero-3-phosphatidylethanolamine lipid bilayers upon peptide binding. Membrane-embedded and membrane-inserted states of the peptide were observed via sum frequency generation vibrational spectroscopy. Circular dichroism, ITC, and ^{31}P NMR data for *Escherichia coli* lipids agree with the hypothesis that strong electrostatic lipid−peptide interactions embrace the peptide at the lipid−water interface and provide the basis for bacterial cell selectivity.

Antimicrobial peptides (AMPs)[1] are produced as a part of host defense mechanisms by various organisms that include microbes, insects, plants, vertebrates, and mammals (*1*−*5*). Most of the antimicrobial peptides are hydrophobic and cationic and exert their activity against pathogens by interacting with target cell membranes (*6*−*8*). An intriguing aspect of AMPs is that these peptides are not toxic to the epithelial and immune cells of the host organism but disrupt the membrane of only microbes and pathogens. The remarkable ability of AMPs to selectively disrupt the membrane of pathogens has been documented (*9*−*18*). However, the exact attributes for target cell membrane selectivity are not clearly understood, partly because of the variance in the primary structure of AMPs and their environment-dependent propensity to adopt secondary conformations.

The membrane activity of linear antimicrobial peptides is generally explained in terms of three distinct steps: (1) an unstructured or partially structured monomeric state in water, (2) membrane-embedded partially structured monomeric or oligomeric state, and (3) inserted across the lipid bilayer as a monomer or bundle. Amphipathic α-helical peptides that exhibit both antimicrobial and hemolytic activities have been demonstrated to insert across the lipid bilayer (*19*−*23*). A subset of AMPs, especially the short peptides, has been reported to exert only antimicrobial activity and low or negligible hemolytic activity without causing substantial membrane disruption (*24*−*30*). Structurally constrained cyclic peptides also exhibit selective adsorption to bacterial membranes (*31*−*33*). Peptide toxins and designer cell-lytic peptides are known to display both antimicrobial and hemolytic properties and insert across the lipid bilayer (*34*−*37*). A significant number of designer peptides have been developed to improve the therapeutic potential of AMPs in general (*37*−*41*). However, toxicity to human cells remains a major concern in the development of therapeutic peptide antibiotics.

[†]This work was supported by National Institutes of Health (NIH) Grants AI054515, GM084018, and RR023597 to A.R. and NIH Grant GM081655-01A2 to Z.C., CRIF-NSF funding for the NMR spectrometer, and the Office of Naval Research (Grant N00014-08-1-1211 for Z.C.). D.K.L. was supported by funds from the Korea Research Foundation (MOEHRD, Basic Research Promotion Funds, KRF-2006-331-C00153).

*To whom correspondence should be addressed. Phone: (734) 647-6572. Fax: (734) 764-3323. E-mail: ramamoor@umich.edu.

[1]Abbreviations: AMP, antimicrobial peptide; CSA, chemical shift anisotropy; CD, circular dichroism; DiPoPE, 1,2-dipalmitoleoyl-*sn*-glycero-3-phosphatidylethanolamine; DSC, differential scanning calorimetry; H_I, normal hexagonal phase; H_{II}, inverted hexagonal phase; ITC, isothermal titration calorimetry; L_α, fluid lamellar phase; MIC, minimum inhibitory concentration; MLVs, multilamellar vesicles; NMR, nuclear magnetic resonance; POPC, 1-palmitoyl-2-oleoyl-*sn*-glycero-3-phosphatidylcholine; POPC-d_{31}, 1-d_{31}-palmitoyl-2-oleoyl-*sn*-glycero-3-phosphatidylcholine; POPG, 1-palmitoyl-2-oleoyl-*sn*-glycero-3-phosphatidylglycerol; POPE, 1-palmitoyl-2-oleoyl-*sn*-glycero-3-phosphatidylethanolamine; SUVs, small unilamellar vesicles.

Published on Web 11/09/2010

Table 1: Determination of Minimal Inhibitory Concentrations of MSI-367 against Microbes

microorganism	expt 1	expt 2	expt 3	expt 4	expt 5	expt 6	MIC (μg/mL)
S. aureus	4	4	4	4	4	8	4 (1.6)[a]
P. aeruginosa	8	8	4	4	8	8	8 (2.8)[a]
E. coli	4	4	2	4	4	8	4 (1.6)[a]
C. albicans	64	64	64	128	64	64	64 (25.8)[a]

[a]Numbers given in parentheses are the MIC values in micromolar.

In the context of AMP-related toxicity, we hypothesize that hemolytic activity can be averted selectively by limiting the peptide−membrane interactions at the lipid−water interface and thereby preventing peptide insertion and membrane lysis.

In this study, we tested our hypothesis using a 21-residue synthetic antimicrobial peptide MSI-367, composed of only three amino acid residues. In this report, we provide evidence of selective permeabilization of a bacterial membrane over a red blood cell membrane. We show the surface binding of the peptide from the lipid order parameters derived from ^{31}P and de-Paked ^{2}H NMR spectra of peptide-incorporated lipid bilayers. Using ^{31}P NMR of mechanically oriented lipid bilayers, we demonstrate the lipid-selective interactions of the peptide. We show the membrane-embedded conformation of the peptide using circular dichroism (CD) measurements. We also show the effect of the membrane-bound peptide on the phase transition (T_H) behavior of lipid vesicles. In addition, we present the enthalpy changes associated with peptide-induced changes in zwitterionic and acidic lipid vesicles. Moreover, we deduce the orientation of the membrane-bound peptide axis using sum frequency generation (SFG) vibrational spectroscopy. Further, the ramifications of this study are discussed in terms of bacterial cell-selective activity stemming from the formation of specific peptide−lipid complexes.

MATERIALS AND METHODS

Materials. All lipids were purchased from Avanti Polar Lipids (Alabaster, AL). Chloroform and methanol were procured from Aldrich Chemical Inc. (Milwaukee, WI). Naphthalene was from Fisher Scientific (Pittsburgh, PA). Buffers were prepared using water obtained from a NANOpure A filtration system. All solvents and reagents were purchased from Bachem, Synthetech Inc., Aldrich Chemical Co., Fisher Scientific, and Protein Technologies. All chemicals were used without further purification. Peptides MSI-78 and MSI-367 were synthesized using standard Fmoc chemistry protocols by Genaera Corp.

Antimicrobial Assay. A doubling dilution series of peptide, beginning with 100 μg/mL, was added to the wells of a sterile 384-well microtiter plate (12 replicates per dilution) and dried overnight in a desiccator box. Bacterial suspensions (10 μL, 10^7 cells/mL) were added to the wells, and the wells were covered with a sterile plastic film, centrifuged briefly to collect the cells in the bottom of the wells, and incubated at 37 °C for 6−36 h, depending upon the rate of growth of the bacterial species. Bacteria were incubated under a normal atmosphere. The terminal cell numbers were determined by the turbidometric method (OD_{600} = 0.02). MICs were set as the lowest concentration of the peptide at which there was no growth above the inoculated level of bacteria ($p < 0.05$; $n = 12$). Values expressed in Table 1 represent $\log_{10}$ growth above inoculated levels.

Hemolysis Assay. The hemolytic activity of the peptides was determined by measuring the hemoglobin released from suspensions of fresh sheep erythrocytes. Red blood cells (Colorado Serum Co., Denver, CO) were centrifuged and washed three times with phosphate-buffered saline [0.15 M NaCl and 0.05 M phosphate buffer (pH 7.4)]. One hundred microliters of red blood cells was added to the wells of a 96-well plate, and then 100 μL of the peptide solution [in PBS (phosphate-buffered saline)] was added to each well. The plates were covered with an adhesive plastic sheet, incubated for 1 h at 37 °C, and centrifuged at 200*g* for 10 min. The absorbance of the supernatants was measured at 414 nm. Zero and one hundred percent levels of hemolysis were determined in PBS and 0.1% Triton X-100, respectively.

Outer Membrane Disruption Assay. The outer membrane permeabilizing ability was investigated using the 1-anilinonaphthalene-8-sulfonic acid (ANS) uptake assay (*41*), on *Escherichia coli* strain BL21(DE3). Bacterial cells from an overnight culture were inoculated into LB medium. Cells from the midlog phase were centrifuged and washed with PBS buffer [10 mM phosphate and 150 mM NaCl (pH 7.4)] and then resuspended in PBS buffer to an OD_{600} of 1.2. To 3.0 mL of the cell suspension in a cuvette was added a stock solution of ANS to a final concentration of 5.0 μM. The degree of membrane disruption as a function of peptide concentration was observed by the increase in fluorescence intensity at ~500 nm.

Circular Dichroism. Small unilamellar vesicles (SUVs) were prepared by sonication. Different lipids in appropriate proportions were dissolved in chloroform, and the clear solution was taken to dryness. PBS buffer [10 mM sodium phosphate, 150 mM NaCl, and 2 mM EDTA (pH 7.4)] was added to dry lipid film and subjected to vortex and sonication to yield a clear dispersion of SUVs. CD spectra were recorded (JASCO spectropolarimeter, model J-715-150S) at 25 °C using samples with peptide:lipid ratios of ~1:100 and ~1:200 in a quartz cuvette (path length of 0.1 cm) over the range from 190 to 250 nm. Contributions from the buffer and SUVs were removed by subtraction of the spectra of the corresponding control samples without peptide. The resultant spectra were normalized for path length and concentration. An aliquot of peptide stock solution was added using a Hamilton syringe to preformed SUVs suspended in PBS buffer and incubated at room temperature for ~5 min to allow equilibrium binding before CD spectra were recorded. The peptide concentration was 74.5 μg/mL.

Solid-State NMR. Mechanically aligned POPC, POPE, POPG, and *E. coli* total lipid bilayers were prepared using the procedure described previously (*42*). Briefly, 4 mg of lipid and an appropriate amount of peptide were dissolved in a $CHCl_3/CH_3OH$ (2:1) mixture. The sample was dried under a stream of nitrogen and dissolved in a $CHCl_3/CH_3OH$ (2:1) mixture containing equimolar quantities of naphthalene. An aliquot of the solution (~300 μL) was spread on two thin glass plates (11 mm × 22 mm × 50 μm, Paul Marienfeld GmbH & Co., Bad Mergentheim, Germany). The samples were air-dried and then kept under vacuum for at least 10 h at 37 °C to remove naphthalene and any residual organic solvents. After being dried, the samples were hydrated at 93% relative humidity using a saturated $NH_4H_2PO_4$ solution for 2−3 days at 37 °C, after which approximately 2 μL of H_2O was misted onto the surface of the lipid−peptide film to increase the water content and therefore the extent of hydration of lipid bilayers in the sample. The glass plates were stacked, wrapped with parafilm, sealed in plastic bags (Plastic Bagmart, Marietta, GA), and then kept at 4 °C for 6−24 h.

^{31}P NMR spectra of mechanically aligned lipid bilayers were obtained from a Varian Infinity 400 MHz solid-state NMR

spectrometer operating at a resonance frequency of 161.979 MHz for the ^{31}P nucleus. A Chemagnetics temperature controller was used to maintain the sample temperature, and each sample was equilibrated at 30 °C for at least 30 min before the experiment was started. The lipid bilayers were positioned in such a way that the bilayer normal was parallel to the external magnetic field axis. A home-built double-resonance probe, which has a four-turn square coil (12 mm × 12 mm × 4 mm) constructed using a 2 mm wide flat wire and a spacing of 1 mm between turns, was used. A typical ^{31}P 90° pulse length of 3.1 μs was used. ^{31}P NMR spectra were recorded using a spin−echo sequence (90°−τ−180°, where τ = 100 μs), a 30 kHz proton-decoupling RF field, a 50 kHz spectral width, and a recycle delay of 3 s. A typical spectrum required the co-addition of 100−1000 transients. The ^{31}P chemical shift spectra are referenced relative to 85% H_3PO_4 on thin glass plates (0 ppm). Data processing was conducted using Spinsight (Chemagnetics/Varian) on a Sun Sparc workstation.

Differential Scanning Calorimetry. Both the peptide and DiPoPE were dissolved in a $CHCl_3$/CH_3OH (2:1) mixture. The solution was dried under a stream of nitrogen and then under high vacuum for several hours. Buffer [10 mM Tris-HCl, 100 mM NaCl, and 2 mM EDTA (pH 7.4)] was added to each sample and each mixture vortexed to resuspend the peptide and lipid. The final concentration of the lipid solution was 10 mg/mL. The solutions were degassed under vacuum for 15 min before the DSC measurements. The heating scan rate was 1 °C/min. The L_α-to-H_{II} transition temperature of lipids was measured on a CSC 6100 Nano II differential scanning calorimeter (Calorimetry Sciences, Provo, UT). The raw data were then converted to molar heat capacity using the CPCalc program available with the calorimeter. In each conversion, the average lipid molecular weight for each sample and a partial specific volume of 0.956 mL/g were used.

Isothermal Titration Calorimetry. The enthalpy of the lipid−peptide mixing reaction was measured using a high-sensitivity isothermal titration calorimeter (TA Instruments, Nano ITC 2G). Peptide and lipid solutions in PBS buffer were degassed under vacuum prior to use. The calorimeter was calibrated as recommended by the manufacturer. The heats of dilution for successive 10 μL injections of the lipid suspension (~7.2 mM) into PBS buffer (pH 7.4) were insignificant compared to the heats of peptide−lipid reaction. The peptide concentration was 5 μM. The heat liberated from successive injections of the lipid was determined by integrating the area under each titration curve using the built-in NanoAnalyze software.

Sum Frequency Generation Experiments. The sum frequency generation (SFG) spectrometer setup used in this study was purchased from EKSPLA. Langmuir−Blodgett and Langmuir−Schaefer (LB/LS) methods (*43*) were used to deposit the proximal and distal leaflets of POPG, respectively (*44*). A CaF_2 prism was attached to a sample holder, and the right-angle face was perpendicularly immersed in the water inside the Langmuir trough. An appropriate amount of a lipid/chloroform solution was then gently spread onto the water surface, and chloroform was allowed to evaporate. The lipid monolayer area was compressed by two barriers at a rate of 5 mm/min until a surface pressure of 34 mN/m was reached. The prism was lifted out of the subphase at a rate of 1 mm/min to obtain a monolayer of lipid on the prism. The right-angle surface of the prism with the monolayer was horizontally lowered to contact again the monolayer deposited on the water surface (with a surface pressure of 34 mN/m) of the trough to form a lipid bilayer. After the formation of the bilayer, the extra lipids at the air−water interface were removed using a micropipet. The bilayer was immersed in water kept in a 2.0 mL reservoir. For peptide−bilayer interaction experiments, a specific volume of the aqueous stock solution of MSI-367 or MSI-78 was injected into the 2.0 mL reservoir to achieve the desired concentration of the peptide. A magnetic microstirrer was used to ensure a homogeneous reservoir concentration. All experiments were conducted at room temperature (~24 °C). SFG amide I spectra were recorded for the peptides associated with the lipid bilayer using *ssp* (*s*-polarized sum frequency signal beam, *s*-visible input beam, and *p*-IR input beam) and *ppp* polarization combinations.

RESULTS

Design of a Cationic, Amphipathic, Linear MSI-367. Because a minimum of 21 residues in the α-helical conformation is required to span the membrane bilayer (*45*), MSI-367 was designed using three repeat units of a weakly membrane active heptapeptide (KFAKKFA) represented by only three amino acids. The hydrophobicity values of Lys, Ala, and Phe (−3.9, 1.8, and 2.8, respectively) are effectively utilized in designing a membrane interface-seeking peptide like MSI-367 with a low aliphatic index (*46*, *47*). With a predicted ~48% helical propensity index (*48*), peptide MSI-367 can be expected to fold into a maximum of five helical turns under favorable conditions. The peptide has nine positively charged lysine residues and, therefore, can preferentially and simultaneously bind to nine negatively charged lipids in membranes such as bacterial and tumor cell membranes. Because alanine is weakly hydrophobic and aromatic residues have a tendency to seek the membrane−water interface, six alanine and six phenylalanine residues were judiciously incorporated to limit the association of the peptide at the lipid−water interface. The overall aliphatic index of the peptide is 28.57 and comparable to those obtained for peptides with demonstrated membrane-selective binding ability (*41*). Also, persistent and transient cation−π interactions between the side chains of lysine and phenylalanine might play a role in modulating the membrane selectivity. Thus, by preventing MSI-367 from assuming a transmembrane orientation, we must be able to retard the formation of a pore structure in the membrane and thereby prevent lysis of the target cell. It is worth mentioning here that non-pore-forming short peptides would be less toxic to mammalian membranes and better candidates for cell targeting and pharmaceutical applications (*1*−*6*).

MSI-367 Exhibits a Broad Spectrum of Antimicrobial and No Hemolytic Activities. Antimicrobial and hemolytic activities were assessed as described previously (*37*, *41*). The minimal inhibitory concentrations (MICs) of MSI-367 against *E. coli*, *Staphylococcus aureus*, *Pseudomonas aeruginosa*, and *Candida albicans* were determined from six independent experiments. MSI-367 exhibits activity against both Gram-positive and Gram-negative bacteria as well as *C. albicans* as shown in Table 1. The reduced activity of MSI-367 against *C. albicans* (higher MIC value compared to those observed for bacteria) suggests either a difference in membrane composition or a mechanism of membrane permeabilization. At concentrations comparable to MIC values of bacteria, MSI-367 did not show any observable hemolytic activity. However, ~20% hemolysis was observed at 100 μg/mL peptide (Figure 1A). Hemolysis at high peptide concentrations has been observed even for amyloid-forming peptides that act on membranes by a different mechanism (*49*). Therefore, an understanding of the biophysical features of MSI-367 that displays cell-selective activity would be useful for the future design of therapeutic peptides.

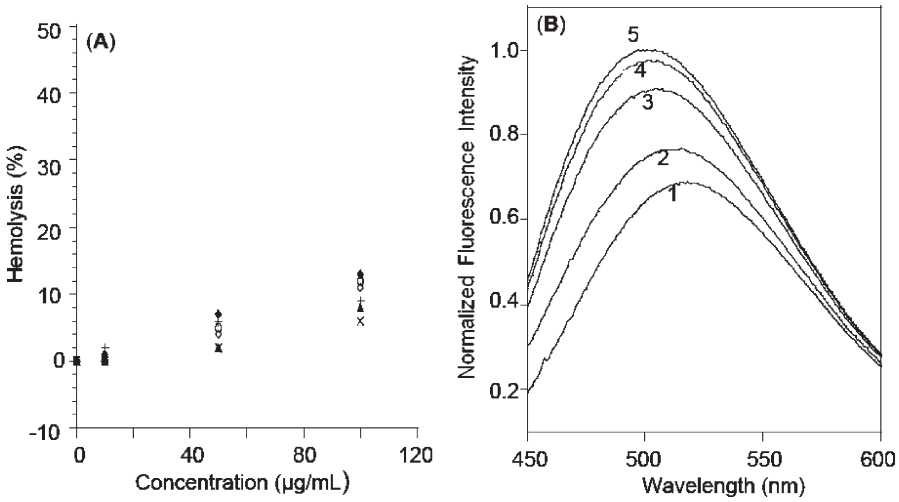

FIGURE 1: (A) Hemolysis profile of MSI-367 in six independent experiments at the indicated concentrations (micrograms per milliliter). Maximum lysis (100%) was observed with 2% Triton X-100. (B) MSI-367 induced the uptake of ANS into the *E. coli* membrane. Fluorescence spectrum of ANS equilibrated with *E. coli* cells (1) and in the presence of 0.67 (2), 1.33 (3), 2.0 (4), and 2.67 μM MSI-367 (5). The *E. coli* cell density, as measured by the OD_{600}, was 1.20. The blue shift in the fluorescence emission maximum indicates the extent of penetration of ANS into the *E. coli* membrane as a function of peptide concentration.

Bacterial Outer Membrane Permeabilization by MSI-367. The effective concentrations required to induce bacterial membrane permeabilization as opposed to the red blood cell membrane would reveal the difference in the mode of interaction of MSI-367 with biomembranes. We assessed the ability of MSI-367 to permeabilize the outer membrane of Gram-negative *E. coli* by measuring the enhancement of the fluorescence intensity of ANS when ANS relocates into the *E. coli* membrane interior (*50*). Being acidic at pH 7.4, ANS can penetrate into the hydrophobic membrane interior only when the membrane is substantially permeabilized. In a typical fluorimetry assay, *E. coli* cells harvested from a midlog phase culture were equilibrated with ANS (5.0 μM) for 5 min and then treated with the indicated concentrations of MSI-367 for 10 min. As shown in Figure 1B, MSI-367 induced the relocation of ANS into the *E. coli* membrane in a concentration-dependent manner. It is imperative to note here that peptide-induced osmotic lysis of *E. coli* cells did not occur during the experiment as the cell density (OD_{600}) of the test sample before and after the addition of the peptide remained comparable. Also, outer membrane permeabilization was observed at concentrations comparable to the MIC against *E. coli* cells. However, consideration of the cell densities used in these two assays points to the fact that much less peptide is required for outer membrane permeabilization (see Materials and Methods). Because the peptide concentrations required for outer membrane permeabilization and killing the bacteria (MIC) are different, peptide-induced changes on membrane bilayers composed of different synthetic lipids and *E. coli* total lipids were studied.

The Secondary Structure of MSI-367 in a Membrane Environment Is Significantly Different from That Observed in Solution. CD is a convenient technique for studying the secondary structure of polypeptides in various media. Because MSI-367 exhibited distinct interactions with different membranes, we examined the effect of lipid vesicles on the structure of MSI-367 using CD experiments. Normalized CD spectra of MSI-367 in trifluoroethanol (TFE), in PBS (pH 7.4), and in the presence of SUVs prepared from POPC and *E. coli* total lipids are shown in Figure 2A. The CD spectrum of MSI-367 in aqueous buffer (trace 1) resembles the one with a largely unordered peptide structure. The positive maximum at ~218 nm and the negative minimum at ~200 nm might be reminiscent of turn conformations (*51*). The spectrum of MSI-367 in neat TFE (trace 4) displays two negative minima at ~222 and ~208 nm suggesting the presence of a regularly folded α-helical conformation, as predicted. However, in the presence of POPC vesicles, the peptide shows a negative minimum at ~204 nm that suggests a random coil conformation, but the low intensity of the band observed at ~204 nm (trace 2) argues against a 100% random coil conformation. Interestingly, the CD spectrum of MSI-367 in *E. coli* lipid vesicles exhibits a broad minimum at ~224 nm (trace 3) suggestive of a β-strand-like conformation. Even though the peptide-induced turbidity changes due to aggregation of vesicles observed during this experiment are in line with the β-strand conformation of the peptide, caution must be exercised while interpreting the CD data as the turbidity of the sample might have distorted the observed profile. Nevertheless, the transition from a random coil to an ordered secondary structure upon interaction with SDS micelles was confirmed from the proton NMR spectra of the peptide (Figure 2B).

MSI-367 Induces Positive Curvature Strain on DiPoPE Lipid Bilayers. Membrane bilayers composed of *E. coli* lipids, POPE and DiPoPE, are known to undergo a transition from L_α to H_I and H_{II} phases above their phase transition temperatures (*52*). Cell-penetrating peptides have been shown to reduce the phase transition temperature of lipid vesicles (*53*). As shown in Figure 3, pure DiPoPE underwent the L_α-to-H_{II} phase transition at ~43 °C. However, when MSI-367 was incorporated into DiPoPE at a peptide:lipid (P:L) ratio of 1:500 (0.2 mol % MSI-367), the transition temperature increased by ~2 °C (Figure 3). The transition temperature increased further when larger amounts of MSI-367 were incorporated (Figure 4, 0.4 mol %). Thus, it appears that even at a P:L ratio of 1:500, MSI-367 induces positive curvature strain and encumbers the L_α-to-H_{II} phase transition of DiPoPE. This observation is consistent with ^{31}P NMR data of POPE lipid bilayers containing MSI-367.

NMR Experiments Reveal MSI-367-Induced Structural Changes in Lipid Bilayers. We used ^{31}P NMR to study the lipid headgroup conformation and ^{2}H NMR of deuterated POPC (POPC-d_{31}) to measure the peptide-induced disorder in the hydrophobic part of the lipid bilayer. To understand how the transient

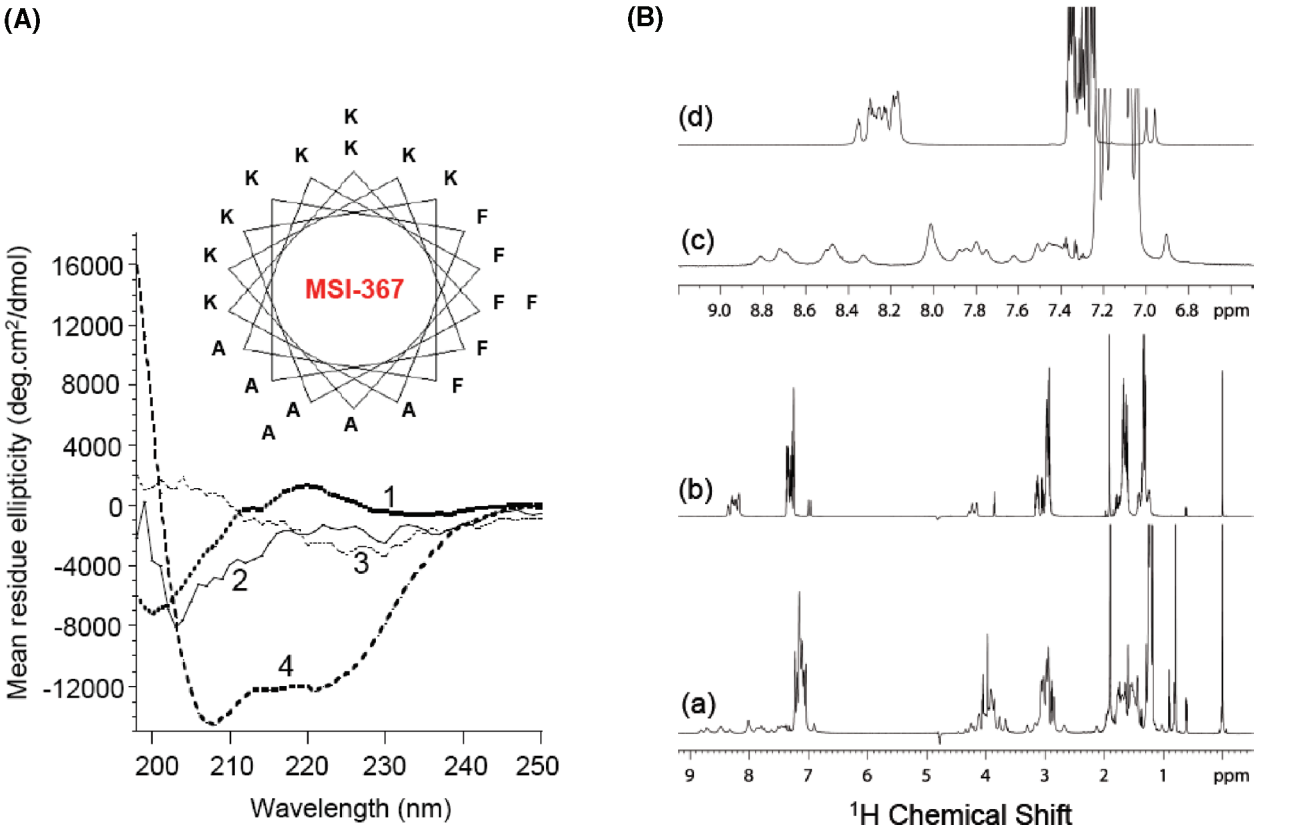

FIGURE 2: (A) Helix wheel representation of MSI-367 and CD spectra of MSI-367 in different media: phosphate-buffered saline (pH 7.4) (1), SUVs of POPC (2), SUVs of *E. coli* total lipids (3), and TFE (4). The peptide concentration was 30 μM. The concentration of POPC was 550 μM, and that of *E. coli* lipids was 840 μM. When all the residues are assumed to be part of the helix, the polar angle subtended by the helix is 154°. (B) ^{1}H NMR spectra of MSI-367: 2.53 mM peptide in 20 mM sodium phosphate buffer (pH 6.0) (traces b and d) obtained from a Bruker (East Lansing, MI) 900 MHz spectrometer or 1.5 mM peptide and 180 mM SDS-d_{23} in 10 mM sodium phosphate buffer (pH 6.0) (traces a and c).

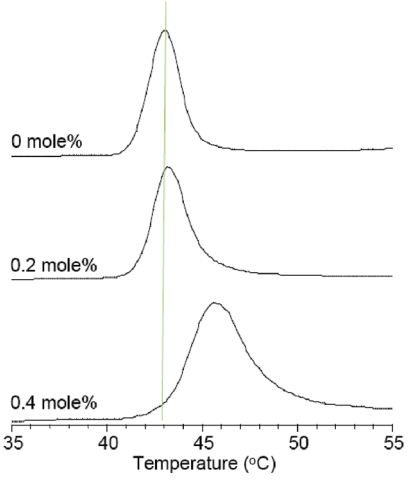

FIGURE 3: DSC thermograms of DiPoPE supplemented with different concentrations of MSI-367. The heating scan rate was 1 °C/min. The vertical dotted line shows the phase transition temperature (T_m = 43 °C) of pure DiPoPE. The phase transition thermograms of DiPoPE containing 0.2 and 0.4 mol % peptide are also shown.

lesions cause leakage, we examined the ^{2}H and ^{31}P NMR spectra of POPC and ^{31}P NMR spectra of POPE, POPG, and *E. coli* total lipid bilayers containing various amounts of MSI-367. de-Paked ^{2}H NMR spectra of pure POPC-d_{31} MLVs and POPC-d_{31} MLVs containing 3 and 5 mol % MSI-367 are shown in Figure 4A. The well-resolved quadrupolar splittings display the characteristic dynamic orders of the methylene (CD_2) units along the lipid acyl chain in the bilayer. As shown in Figure 4B, the differences in order parameters derived from the observed quadrupolar splittings are greatest for the CD_2 groups closer to the lipid headgroup region and show a decreasing trend along the acyl chain toward a minimum for the other end of the chain, implying a strong localized effect at the water−bilayer interface.

To determine the peptide-induced structural changes in the water−bilayer interface region, we obtained ^{31}P NMR spectra from mechanically aligned lipid bilayers. Figure 5 shows the ^{31}P NMR spectra of oriented POPC, POPG, and POPE lipid bilayers supplemented with various amounts of MSI-367. ^{31}P NMR spectra of pure lipid bilayers display a narrow peak at ~31 ppm (Figure 5, top traces), indicating that almost all lipids are aligned with the bilayer normal parallel to the external magnetic field axis. However, ^{31}P NMR spectra of lipid bilayers supplemented with increasing amounts of MSI-367 show a concentration-dependent shift toward the high-field region of the spectrum and broadening of the resonance at ~31 ppm. Incorporation of 15 mol % MSI-367 appears to disrupt the planar bilayer integrity substantially and promote nonplanar structures (*54*, *55*). Thus, the peptide-induced membrane disruption seems to depend partly on the concentration regime, which determines the type of peptide−lipid complex at the water−bilayer interface.

Because phosphatidylethanolamine is the major lipid in the *E. coli* membrane (*56*), understanding the interaction of MSI-367 with this lipid would provide insights into its mechanism of antibacterial action. ^{31}P NMR spectra of *E. coli* lipid bilayers supplemented with increasing amounts of MSI-367 are shown in Figure 6 and compared with that of bilayers containing pexiganan (MSI-78).

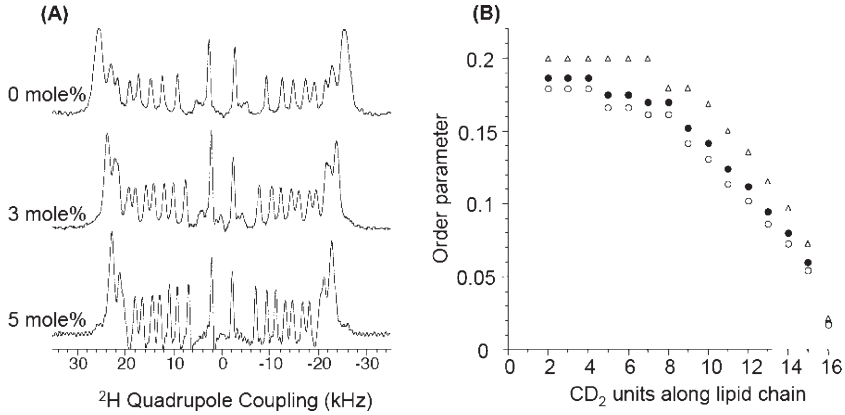

FIGURE 4: (A) de-Paked ^{2}H quadrupole coupling spectra of POPC-d_{31} MLVs and POPC-d_{31} MLVs supplemented with 3 and 5 mol % MSI-367. (B) Plot of order parameter vs lipid acyl chain carbon number: POPC-d_{31} (△), POPC-d_{31} with 3 mol % MSI-367 (●), and POPC-d_{31} with 5 mol % MSI-367 (○).

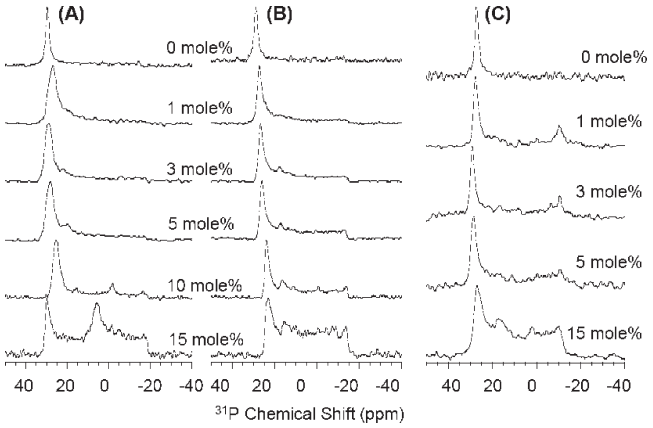

FIGURE 5: ^{31}P chemical shift spectra of aligned POPC (A), POPE (B), and POPG (C) lipid bilayers in the presence and absence of MSI-367. The peptide concentrations are indicated. Each spectrum was obtained from 4 mg of lipids and required 100−1000 transients.

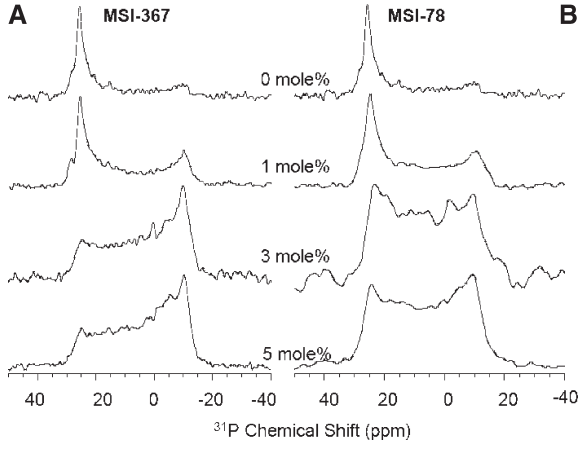

FIGURE 6: ^{31}P chemical shift spectra of aligned *E. coli* lipid bilayers in the presence and absence of MSI-367 (A) and MSI-78 (B). The peptide concentrations are indicated. Each spectrum was obtained from 4 mg of lipids and required 100−1000 transients.

Pexiganan, a well-studied peptide antibiotic for diabetic foot ulcers, displays bactericidal activity (*10*). In the lower concentration regime (3 mol %), both pexiganan and MSI-367 seem to exert similar effects on *E. coli* lipid bilayers. However, distinctly different effects are seen at higher concentrations (≥5 mol %) of these peptides. While pexiganan appears to promote the formation of nonlamellar structures, MSI-367 clearly transforms the aligned planar bilayers into unaligned multilamellar structures. The differential activity exhibited by these peptides might underscore the structural differences between the different types of lipid−peptide complexes formed. Because pexiganan is a bactericidal peptide, MSI-367 is likely to exert its antimicrobial activity by a different mechanism.

The Enthalpy of Interaction of MSI-367 with Lipids Explains Its Bacterial Selectivity. Because partitioning of hydrophobic residues into lipid bilayers usually results in a net negative enthalpy and partial insertion of peptides leads to a net positive enthalpy (*57*), we measured the enthalpy changes associated with the interactions of MSI-367 with POPC and *E. coli* lipid vesicles, to assess any lipid specific interactions. The heat capacity changes measured in microwatts from successive titrations of lipid into peptide at 25 °C are presented in Figure 7 (top panel). The variation in enthalpy as a function of lipid:peptide ratio is also given in Figure 7 (bottom panel). A qualitative analysis of Figure 7 reveals the two distinct modes of interaction of MSI-367 with zwitterionic POPC and acidic *E. coli* lipid vesicles. While the thermogram representing titrations of MSI-367 with POPC (Figure 7A) suggests a two-state binding to lipid vesicles, the interaction of the peptide with *E. coli* lipid vesicles leads to membrane fusion and aggregation (Figure 7B). It is imperative to note here that visible small aggregates formed during the titrations settled down upon standing as a single large lump probably because of the exposure of hydrophobic moieties in the smaller aggregates. The two distinct modes of interaction of MSI-367 with zwitterionic POPC and anionic *E. coli* lipid vesicles clearly explain the bacterial cell-selective activity of the peptide.

Membrane Surface Orientation of MSI-367 Revealed by SFG Experiments. Though ^{31}P and ^{2}H solid-state NMR experiments revealed the membrane surface association of MSI-367, it would be valuable to determine the membrane orientation of the peptide at a lower peptide concentration. Therefore, the direct observation of monolayer surface specific interactions of the peptide observed in sum frequency generation (SFG) was utilized in this study. To gain more insight into the membrane orientation of MSI-367, we used MSI-78 as a reference peptide. The SFG spectra of the POPG bilayer in contact with an MSI-367 or MSI-78 solution with a concentration of 0.8 μM are shown in Figure 8 for a comparison. Strong SFG signals and the fitted signal strength ratio of the *ppp* and *ssp* amide I spectra (χ_{ppp}/χ_{ssp}) obtained for MSI-78 (Figure 8A) indicate that MSI-78 strongly interacts with the POPG bilayer. The χ_{ppp}/χ_{ssp} ratio of 1.2

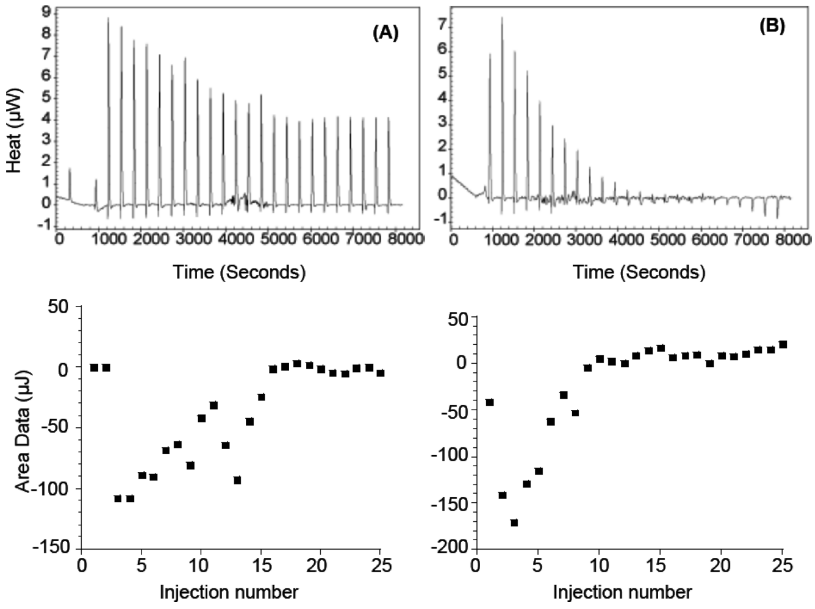

FIGURE 7: Titration calorimetry thermograms of titrations of POPC (A) and *E. coli* (B) lipid into peptide. Aliquots of a 10 μL lipid solution (~20 mM) were added to the peptide solution (5 μM) in the reaction cell (V = 1.0 mL). The top panel shows the calorimeter traces. The enthalpies of reaction, which is calculated by integration of the calorimeter traces, are given in the bottom panel.

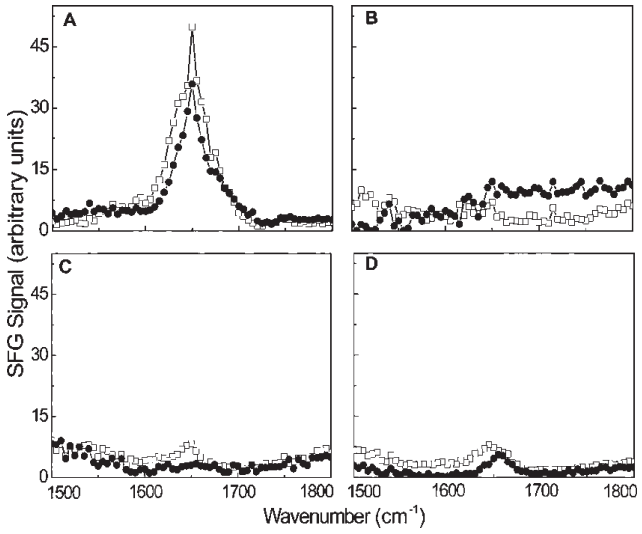

FIGURE 8: SFG vibrational spectra. Amide I signals obtained from the single POPG bilayer in contact with 0.8 μM MSI-78 (A) or 0.8 (B), 1.2 (C), and 2.0 μM MSI-367 solutions (D): (□) *ppp* spectra and (■) *ssp* spectra. While there is no signal observed from 0.8 μM MSI-367, a low-intensity *ppp* signal was observed for 1.2 μM peptide.

indicates the existence of more than one distinct orientation: some are inserted into the bilayer, and others are oriented on the lipid bilayer surface (*58*) as shown in Figure 9. The membrane-inserted orientation, or lining of the toroidal pore surface, of MSI-78 is seen even for a concentration of 0.4 μM (data not shown). On the other hand, no discernible SFG signals are observed when the POPG bilayer is in contact with a 0.8 μM MSI-367 solution (Figure 8B). Our data suggest that MSI-367 molecules are either not associated with the bilayer or oriented on the lipid bilayer surface. When the MSI-367 concentration was increased to 1.2 μM, the *ssp* signal was still not observed, and a weak SFG *ppp* signal (3 or 4 times stronger than the noise) was detected (Figure 8C). Even when a 1.2 μM solution of MSI-367 is in contact with the lipid bilayer, only the *ppp* signal and not the *ssp* signal is seen. The SFG signal intensity of 2.0 μM MSI-367 is, also, much weaker that of 0.8 μM MSI-78 (Figure 8A,D). Thus, our data clearly indicate that there is no insertion of MSI-367 into the hydrophobic core of the POPG bilayer. Both MSI-78 and MSI-367 have the same number of amino acids, the same helix propensity, and nine positively charged residues. Hence, it is likely that the high aliphatic index (93.18) of MSI-78 favors insertion into the lipid bilayer, while the low aliphatic index (28.57) of MSI-367 allows membrane interfacial localization of the peptide as suggested by NMR experiments.

The relationship between tilt angle (θ) and χ_{ppp}/χ_{ssp} is shown in Figure 9 in terms of different states of membrane-bound peptides. The estimated *ppp*/*ssp* ratio obtained by curve fitting for 0.8 μM MSI-78 is 1.2 and falls outside the curve simulated for a single helical orientation suggesting a multiple-helix orientation for the membrane-bound peptide as shown in Figure 9 (right panel). On the other hand, the only *ppp* signal observed for 1.2 μM MSI-367 with a *ppp*/*ssp* signal strength ratio of ~2, very different from that observed for MSI-78, suggests that the alignment of the MSI-367 peptide with the POPG membrane is very different from that observed for MSI-78. This significant difference between these two peptides can be attributed to the structural differences between them and explains the bacterial membrane selectivity of MSI-367.

DISCUSSION

The Design of Highly Potent and Selective Antimicrobial Peptides Is Essential. Increasing bacterial resistance toward conventional antibiotic compounds is a major problem, and therefore, there is an urgent need for the development of compounds that could act via different types of mechanisms. Though the naturally occurring antimicrobial peptides with a broad spectrum of antibacterial activities are promising potential candidates for overcoming this problem, the large amount of peptide needed to kill bacteria is a major concern. To this end, several different strategies have been utilized to improve the potency and expand the activity spectrum of antimicrobial peptides. Similarly, efforts have been directed toward reducing the cytotoxicity of cytolytic peptides. They include identification of the minimal fragment for antimicrobial activity (*41*, *59*), substitution of specific residues to reduce hemolytic activity (*59*, *60*), total or partial

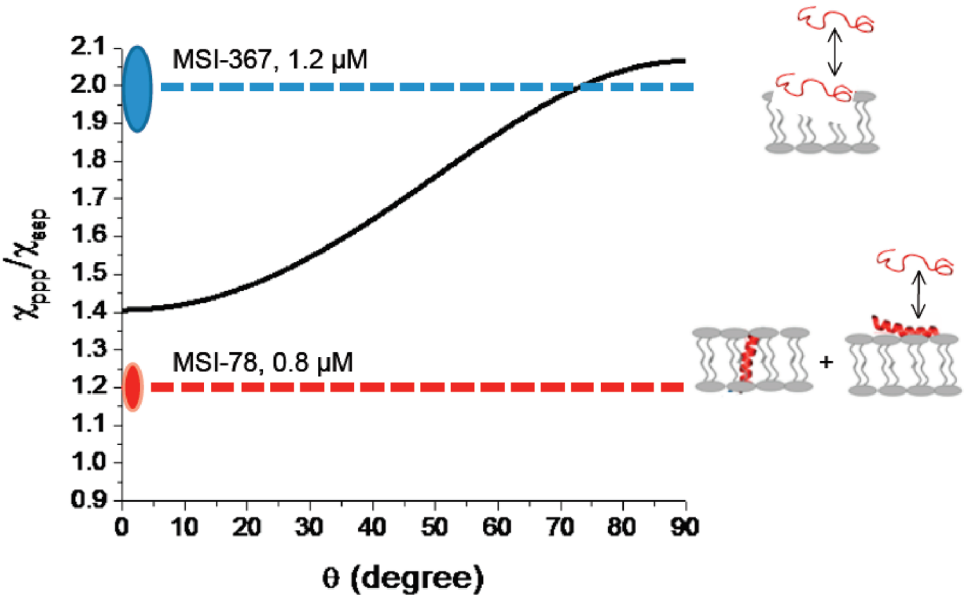

FIGURE 9: Relationship between the SFG *ppp*/*ssp* signal strength ratio and the tilt angle (θ) of a helical peptide by assuming an identical orientation relative to the lipid bilayer normal (solid line). Experimentally measured data points are shown for 0.8 μM MSI-78 and 1.2 μM MSI-367.

replacement with unusual and D-amino acids (*14*, *61*), use of retroenantiomeric analogues (*62*), and cyclization and linearization of natural peptide antibiotics (*37*, *63*).

MSI-367 Is a Suitable Antibacterial Candidate with a Very High Bacterial Selectivity. In this study, we have designed a synthetic AMP to evaluate the biophysical parameters required for selective activity against only bacteria and fungi, and not against human red blood cells. As predicted, MSI-367 shows activity against both bacteria and fungi (Table 1). It also permeabilizes the bacterial outer membrane (Figure 1). In the observed range of MIC values, the peptide does not exhibit any significant hemolytic activity, suggesting a nonlytic killing mechanism against bacteria (*64*). Although peptide-induced membrane permeabilization appears to be critical in eliciting the antimicrobial activity, a comparison of peptide concentrations and *E. coli* cell densities used for MIC determination (Table 1) and outer membrane permeabilization (Figure 1) reveals a role for other factors in killing the bacterium. The lipid:protein ratio at the budding sites on the *E. coli* membrane has been reported to be higher than that for the whole membrane. The protein-depleted budding sites might turn into soft sites for peptide-induced outer membrane permeabilization. This may explain the outer membrane permeabilization observed at concentrations lower than the MIC.

The Location of MSI-367 at the Membrane−Water Interface Suppresses Its Hemolytic Activity. Random coil-to-α-helix conformational transitions upon binding to lipid membranes have been observed for several antimicrobial peptides (*65*). In the membrane mimicking solvent TFE, MSI-367 displays an α-helical conformation (Figure 2A, trace 4) that is consistent with the predicted amphipathic structure resulting from the segregation of hydrophilic and hydrophobic amino acids along the helical axis. Although the peptide has the intrinsic helical propensity, a qualitative analysis of the CD spectra of MSI-367 in the presence of POPC and *E. coli* lipid vesicles reveals only subtle variations in the conformation upon binding (Figure 2A, traces 2 and 3). However, a comparison of chemical shift values for amide NH protons of MSI-367 in aqueous buffer (pH 6.0) and in the presence of 200 mM SDS-d_{25} micelles (Figure 2B) suggests substantial changes in the secondary structure of the peptide. When the peptide:SDS ratio was ~1:10, the peptide−SDS complex aggregated to form a precipitate. When larger amounts of SDS were added, the solution became clear. It is important to note here that MSI-367 induced *E. coli* lipid aggregation during CD measurements, suggesting interfacial association of the peptide. Similar behaviors have been observed with AMPs such as indolicidin and tritrypticin. These peptides are rich in aromatic residues and bind only to the membrane interface (*66*, *67*).

^{2}H NMR experiments were used to measure the peptide-induced effect on the hydrophobic core of lipid bilayers. Addition of MSI-367 decreases the order parameter in a concentration-dependent manner (Figure 4). The changes in the acyl chain order parameter suggest that the peptide binding induces disorder mainly in the interface region of POPC bilayers, and maximal disorder is observed only near the glycerol backbone of the lipid. Negligible changes were observed in the order parameters of CD_2 groups near the terminal methyl group of the lipid that is consistent with the bilayer surface orientation of the peptide (*50*). DiPoPE and PE rich *E. coli* lipids have a tendency to form the inverted hexagonal phase with a negative curvature at higher temperatures because of their small headgroup size relative to the length of the acyl chain. Repression of the L_α-to-H_{II} transition by membrane active peptides has been explained in terms of their surface-bound states (*68*). Similarly, mitigation of the L_α-to-H_{II} transition in DiPoPE liposomes by MSI-367 at a low P:L ratio (Figure 3) observed in this study can be expected from the surface-embedded peptide molecules. Thus, both ^{2}H NMR and DSC studies point to a surface embedded against a transmembrane orientation of the membrane-bound peptide. This prediction is also consistent with the observed changes in the ^{31}P NMR spectra of mechanically aligned bilayers containing MSI-367 (Figure 5A−C). In addition, the peptide-induced lamellar-to-inverted hexagonal phase transition clearly discernible in the case of *E. coli* lipid bilayers (Figure 6A) is in excellent agreement with the DSC data for the synthetic DiPoPE lipid. Such transitions are not observed for a cell lytic antimicrobial peptide MSI-78 (Figure 6B). This unique behavior of MSI-367 is consistent with the *E. coli* outer membrane permeabilizing ability and nonhemolytic nature of the peptide at the MIC.

The selective permeability of the bacterial membrane can be expected from the peptide's ability to induce aggregation of *E. coli* lipids (observed during CD and ITC measurements) and SDS micelles at a P:L ratio of ~1:10 (observed during ^{1}H NMR measurements). Under these conditions, the antimicrobial peptide MSI-78 did not induce lipid aggregation, consistent with its α-helix structure and toroidal pore complex in lipid bilayers (*68*, *69*). ITC thermograms obtained from titrations of lipid into peptide indicate a weak binding affinity for POPC vesicles (Figure 7A) and are in agreement with CD and ^{31}P NMR spectra of MSI-367 in the presence of POPC. However, titrations of *E. coli* lipid vesicles into an MSI-367 solution result in a thermogram indicative of both endothermic and exothermic processes (Figure 7B). While an exothermic process is expected from peptide−lipid interactions, the endothermic process can arise only from the loss of internal energy (*54*, *57*) of the system. Such a loss of internal energy could arise from the exposure of hydrophobic groups and/or a transition from lipid bilayer to lamellar structures (*54*, *57*). The peptide-induced lamellar-to-inverted hexagonal phase transition (Figure 6C) observed in *E. coli* lipid bilayers is in agreement with the endo- and exothermic transitions seen in the thermogram (Figure 7B).

Antimicrobial peptides indolicidin and tritrypticin are rich in aromatic residues and bind to the lipid membrane interface (*66*, *67*). These peptides have been shown to induce lipid aggregation at certain P:L ratios. Because MSI-367 contains six aromatic residues and nine lysine residues, the lipids can effectively embrace the peptide at the lipid−water interface. Membrane-embedded peptide might then induce lipid aggregation, which has been shown in the cases of indolicidin and tritrypticin (*66*, *67*). A comparison of SFG data (Figure 8) on POPG-bound MSI-367 and MSI-78 clearly discloses the surface-embedded orientation of nonhemolytic MSI-367 and the membrane insertion of hemolytic MSI-78 (*70*). Despite the fact that both MSI-367 and MSI-78 are cationic and have intrinsic helix propensity and the required number of amino acids to form a transmembrane channel structure, it appears that the inability of MSI-367 to insert across the lipid bilayer makes it nonhemolytic. The hemolytic activity observed at very high concentrations (> 100 μg/mL) of MSI-367 might be similar to the toxicity observed with peptide amyloids in which preformed peptide aggregates disrupt the cell membrane by an unknown mechanism. At higher concentrations of the peptide, binding of MSI-367 to negatively charged lipids and the disruption of the bilayer structure may involve the formation of inverted micelles (*54*, *57*). The proposed model (Figure 9) for antimicrobial activity of MSI-367 includes a nonlytic peptide−lipid complex in which the peptide lies on the membrane surface in such a way that the lysine side chains are stretched out and the aromatic residues intercalated between the acyl chains at the water−bilayer interface. In this orientation, MSI-367 may induce a positive curvature strain that mitigates the formation of the H_{II} phase (Figure 3). This model also explains the peptide-induced changes in the phosphate headgroup conformation (Figures 5 and 6) and the acyl chain disorder near the headgroups (Figure 4).

CONCLUSION

The nonlytic antimicrobial activity observed against *E. coli* at ~1.6 μM could be explained in terms of the moderate aliphatic index and the nine cationic residues of MSI-367 that confer membrane−water interfacial localization of the peptide as charged molecules cannot cross the lipid bilayer by passive diffusion because of the high Born energy penalty encountered in a medium of low dielectricity (*71*). ^{31}P NMR data of *E.coli* lipid bilayers clearly indicate the formation of unaligned multilamellar lipid structures and suggest that the toroidal-type pore mechanism is unlikely. ^{2}H NMR, DSC, and SFG studies confirm the lipid bilayer interfacial localization of MSI-367. Taken together, our results suggest that limiting the action of antimicrobial peptides to the membrane−water interface has the advantage of improving the therapeutic potential of AMPs as the cell-lytic peptides are not the desirable candidates because of their toxicity.

ACKNOWLEDGMENT

We thank Dr. Anmin Tan for help with fluorescence experiments and Dr. Subramanian Vivekanandan for recording proton NMR spectra of MSI-367. We thank the biomolecular 900 MHz NMR facility at East Lansing, MI.

REFERENCES

1. Giuliani, A., Pirri, G., and Nicoletto, S. F. (2007) Antimicrobial peptides: An overview of a promising class of therapeutics. *Cent. Eur. J. Biol. 2*, 1–33.
2. Zasloff, M. (2002) Antimicrobial peptides of multicellular organisms. *Nature 415*, 389–395.
3. Shai, Y., Makovitzky, A., and Avrahami, D. (2006) Host defense peptides and lipopeptides: Modes of action and potential candidates for the treatment of bacterial and fungal infections. *Curr. Protein Pept. Sci. 7*, 479–486.
4. Hancock, R. E. W., and Sahl, H.-G. (2006) Antimicrobial and host-defense peptides as new anti-infective therapeutic strategies. *Nat. Biotechnol. 24*, 1551–1557.
5. Diamond, G., Beckloff, N., Weinberg, A., and Kisich, K. O. (2009) The roles of antimicrobial peptides in innate host defense. *Curr. Pharm. Des. 15*, 2377–2392.
6. Dhople, V., Krukemeyer, A., and Ramamoorthy, A. (2006) The human β-defensin-3, an antibacterial peptide with multiple biological functions. *Biochim. Biophys. Acta 1758*, 1499–1512.
7. Bhattacharjya, S., and Ramamoorthy, A. (2009) Multifunctional host defense peptides: Functional and mechanistic insights from NMR structures of potent antimicrobial peptides. *FEBS J. 276*, 6465–6473.
8. Epand, R. F., Maloy, L., Ramamoorthy, A., and Epand, R. M. (2010) Amphipathic helical cationic antimicrobial peptides promote rapid formation of crystalline states in the presence of phosphatidylglycerol: Lipid clustering in anionic membranes. *Biophys. J. 98*, 2564–2573.
9. Matsuzaki, K., Sugishita, K., Fujii, N., and Miyajima, K. (1995) Translocation of a channel-forming antimicrobial peptide, magainin 2, across lipid bilayers by forming a pore. *Biochemistry 34*, 6521–6526.
10. Ge, G., MacDonald, D. L., Holroyd, K. J., Thornsberry, C., Wexler, H., and Zasloff, M. (1999) *In vitro* antibacterial properties of pexiganan, an analog of magainin. *Antimicrob. Agents Chemother. 43*, 782–788.
11. Zhang, L., and Falla, T. J. (2009) Host defense peptides for use as potential therapeutics. *Clin. Dermatol. 27*, 485–494.
12. Liu, Z., Young, A. W., Hu, P., Rice, A. J., Zhou, C., Zhang, Y., and Kallenbach, N. R. (2007) Turning the membrane selectivity of antimicrobial peptides by using multivalent design. *ChemBioChem 8*, 2063–2065.
13. Glukhov, E., Stark, M., Burrows, L. L., and Deber, C. M. (2005) Basis for Selectivity of Cationic Antimicrobial Peptides for Bacterial Versus Mammalian Membranes. *J. Biol. Chem. 280*, 33960–33967.
14. Zhu, W. L., Nan, Y. H., Hahm, K.-S., and Shin, S. Y. (2007) Cell selectivity of an antimicrobial peptide melittin diastereomer with D-amino acid in the leucine zipper sequence. *J. Biochem. Mol. Biol. 40*, 1090–1094.
15. Lu, J.-X., Blazyk, J., and Lorigan, G. A. (2006) Exploring membrane selectivity of the antimicrobial peptide KIGAKI using solid-state NMR spectroscopy. *Biochim. Biophys. Acta 1758*, 1303–1313.
16. Eckert, R., Qi, F., Yarbrough, D. K., He, J., Anderson, M. H., and Wenyuan, S. (2006) Adding selectivity to antimicrobial peptides: Rational design of a multidomain peptide against *Pseudomonas* spp. *Antimicrob. Agents Chemother. 50*, 1480–1488.
17. Gottler, L., and Ramamoorthy, A. (2009) Membrane Orientation, Mechanism, and Function of Pexiganan: A Highly Potent Antimicrobial Peptide Designed from Magainin. *Biochim. Biophys. Acta 1788*, 1680–1686.

18. Marsh, E. N. G., Buer, B. C., and Ramamoorthy, A. (2009) Fluorine: A new element in the design of membrane-active peptides. *Mol. BioSyst. 5*, 1143–1147.
19. Bringezu, F., Wen, S., Dante, S., Hauss, T., Majerowicz, M., and Waring, A. (2007) The insertion of the antimicrobial peptide dicynthaurin monomer in model membranes: Thermodynamics and structural characterization. *Biochemistry 46*, 5678–5686.
20. Pistolesi, S., Pogni, R., and Feix, J. B. (2007) Membrane insertion and bilayer perturbation by antimicrobial peptide CM15. *Biophys. J. 93*, 1651–1660.
21. Lee, T. H., Hall, K. N., Swann, M. J., Popplewell, J. F., Unabia, S., Park, Y., Hahm, K. S., and Aguilar, M. I. (2010) The membrane insertion of helical antimicrobial peptides from the N-terminus of *Helicobacter pylori* ribosomal protein L1. *Biochim. Biphys. Acta 1798*, 544–557.
22. Ramamoorthy, A., Lee, D. K., Narasimhaswamy, T., and Nanga, R. P. R. (2010) Cholesterol reduces pardaxin's dynamics: A barrel-stave mechanism of membrane disruption investigated by solid-state NMR. *Biochim. Biophys. Acta 1798*, 223–227.
23. Ramamoorthy, A. (2009) Beyond NMR spectra of antimicrobial peptides: Dynamical images at atomic resolution and functional insights. *Solid State Nucl. Magn. Reson. 35*, 201–207.
24. Serrano, G. N., Zhanel, G. G., and Schweizer, F. (2009) Antibacterial Activity of Ultrashort Cationic Lipo-β-Peptides. *Antimicrob. Agents Chemother. 53*, 2215–2217.
25. Gehman, J. D., Luc, F., Hall, K., Lee, T.-H., Boland, M. P., Pukala, T. L., Bowie, J. H., Aguilar, M., and Separovic, F. (2008) Effect of antimicrobial peptides from Australian tree frogs on anionic phospholipid membranes. *Biochemistry 47*, 8557–8565. Strøm, M. B., Rekdal, Ø., and Svendsen, J. S. (2002) Antimicrobial activity of short arginine- and tryptophan-rich peptides. *J. Pept. Sci. 8*, 431–437.
26. Blondelle, S. E., Takahashi, E., Dinh, K. T., and Houghten, R. (1995) The antimicrobial activity of hexapeptides derived from synthetic combinatorial libraries. *J. Appl. Microbiol. 78*, 39–46.
27. Shamova, O., Orlov, D., Stegemann, C., Czihal, P., Hoffmann, R., Brogden, K., Kolodkin, N., Sakuta, G., Tossi, A., Sahl, H.-G., Kokryakov, V., and Lehrer, R. I. (2009) A novel proline-rich antimicrobial peptide from goat leukocytes. *Int. J. Pept. Protein Res. 15*, 108–119.
28. Chen, C., Pan, F., Zhang, S., Hu, J., Cao, M., Wang, J., Xu, H., Zhao, X., and Lu, J. R. (2010) Antibacterial Activities of Short Designer Peptides: A Link between Propensity for Nanostructuring and Capacity for Membrane Destabilization. *Biomacromolecules 11*, 402–411.
29. Dartois, V., Sanchez-Quesada, J., Cabezas, E., Chi, E., Dubbelde, C., Dunn, C., Granja, J., Gritzen, C., Weinberger, D., Ghadiri, M. R., Thomas, R., and Parr, T. R., Jr. (2005) Systemic antibacterial activity of novel synthetic cyclic peptides. *Antimicrob. Agents Chemother. 49*, 3302–3310.
30. Fernandez-Lopez, S., Kim, H.-S., Choi, E. C., Delgado, M., Granja, J. R., Khasanov, A., Kraehenbuehl, K., Long, G., Weinberger, D. A., Wilcoxen, K. M., and Ghadiri, M. R. (2001) Antibacterial agents based on the cyclic D,L-α-peptide architecture. *Nature 412*, 452–455.
31. Ganz, T. (2003) Defensins: Antimicrobial peptides of innate immunity. *Nat. Rev. Immunol. 3*, 710–720.
32. Abuja, P. M., Zenz, A., Trai, M., Craik, D. L., and Lohner, K. (2004) The cyclic antimicrobial peptide RTD-1 induces stabilized lipid-peptide domains more efficiently than its open-chain analogue. *FEBS Lett. 566*, 301–306.
33. Thennarasu, S., Lee, D. K., Poon, A., Kawulka, K. E., Vederas, J. C., and Ramamoorthy, A. (2005) Membrane permeabilization, orientation, and antimicrobial mechanism of subtilosin A. *Chem. Phys. Lipids 137*, 38–51.
34. Papo, N., and Shai, Y. (2003) New lytic peptides based on the D,L-amphipathic helix motif preferentially kill tumor cells compared to normal cells. *Biochemistry 42*, 9346–9354.
35. Vad, B. S., Bertelsen, K., Johansen, C. H., Pedersen, J. M., Skrydstrup, T., Nielsen, N. C., and Otzen, D. E. (2010) Pardaxin Permeabilizes Vesicles More Efficiently by Pore Formation than by Disruption. *Biophys. J. 98*, 576–585.
36. Asthana, N., Yadavand, S. P., and Ghosh, J. K. (2004) Dissection of antibacterial and toxic activity of melittin: A leucine zipper motif plays a crucial role in determining its hemolytic activity but not antibacterial activity. *J. Biol. Chem. 279*, 55042–55050.
37. Ramamoorthy, A., Thennarasu, S., Tan, A., Gottipati, K., Sreekumar, S., Heyl, D. L., An, F. Y., and Shelburne, C. E. (2006) Deletion of all cysteines in tachyplesin I abolishes hemolytic activity and retains antimicrobial activity and lipopolysaccharide selective binding. *Biochemistry 45*, 6529–6540.
38. Gottler, L. M., de la Salud Bea, R., Shelburne, C. E., Ramamoorthy, A., and Marsh, E. N. (2008) Using Flourous Amino Acids to Probe the Effects of Changing Hydrophobicity on the Physical and Biological Properties of the β-Hairpin Antimicrobial Peptide Protegrin-1. *Biochemistry 47*, 9243–9250.
39. Chen, Y., Mant, C. T., Farmer, S. W., Hancock, R. E. W., Vasil, M. L., and Hodges, R. S. (2005) Rational design of α-helical antimicrobial peptides with enhanced activities and specificity/therapeutic index. *J. Biol. Chem. 280*, 12316–12329.
40. Scott, R. W., DeGrado, W. F., and Tew, G. N. (2008) *De novo* designed synthetic mimics of antimicrobial peptides. *Curr. Opin. Biotechnol. 19*, 620–627.
41. Thennarasu, S., Tan, A., Penumatchu, R., Shelburne, C. E., Heyl, D. L., and Ramamoorthy, A. (2010) Antimicrobial and membrane disrupting activities of a peptide derived from the human cathelicidin antimicrobial peptide LL37. *Biophys. J. 98*, 248–257.
42. Hallock, K. J., Henzler-Wildman, K., Lee, D.-K., and Ramamoorthy, A. (2002) An innovative procedure using a sublimable solid to align lipid bilayers for solid-state NMR studies. *Biophys. J. 82*, 2499–2503.
43. Wang, J., Chen, C., Buck, S. M., and Chen, Z. (2001) Molecular chemical structure on poly(methyl methacrylate) (PMMA) surface studied by sum frequency generation (SFG) vibrational spectroscopy. *J. Phys. Chem. B 105*, 12118–12125.
44. Nguyen, K. T., Le Clair, S. V., Ye, S. J., and Chen, Z. (2009) Molecular interactions between magainin 2 and model membranes *in situ*. *J. Phys. Chem. B 113*, 12358–12363.
45. Castano, S., Cornut, I., Büttner, K., Dasseux, J. L., and Dufourcq, J. (1999) The amphipathic helix concept: Length effects on ideally amphipathic LiKj(i = 2j) peptides to acquire optimal hemolytic activity. *Biochim. Biophys. Acta 1416*, 161–175.
46. Kyte, J., and Doolittle, R. F. (1982) A simple method for displaying the hydropathic character of a protein. *J. Mol. Biol. 157*, 105–132.
47. Ikai, A. J. (1980) Thermostability and aliphatic index of globular proteins. *J. Biochem. 88*, 1895–1898.
48. Garnier, J., Gibrat, J.-F., and Robson, B. (1996) GOR method for predicting protein secondary structure from amino acid sequence. *Methods Enzymol. 266*, 540–553.
49. Yoshiike, Y., Kayed, R., Milton, S., Takashima, A., and Glabe, C. (2007) Pore-forming proteins share structural and functional homology with amyloid oligomers. *NeuroMol. Med. 9*, 270–275.
50. Thennarasu, S., Lee, D.-K., Tan, A., Prasad Kari, U., and Ramamoorthy, A. (2005) Antimicrobial activity and membrane selective interactions of a synthetic lipopeptide MSI-843. *Biochim. Biophys. Acta 1711*, 49–58.
51. Thennarasu, S., and Nagaraj, R. (1997) Solution conformations of peptides representing the sequence of the toxin pardaxin and analogues in trifluoroethanol-water mixtures: Analysis of CD spectra. *Biopolymers 41*, 635–645.
52. Siegel, D. P., and Epand, R. M. (2000) Effect of influenza hemagglutinin fusion peptide on lamellar/inverted phase transitions in dipalmitoleoylphosphatidylethanolamine: Implications for membrane fusion mechanisms. *Biochim. Biophys. Acta 1468*, 87–98.
53. Alves, I. D., Goasdoué, N., Correia, I., Aubry, S., Galanth, C., Sagan, S., Lavielle, S., and Chassaing, G. (2008) Membrane interaction and perturbation mechanisms induced by two cationic cell penetrating peptides with distinct charge distribution. *Biochim. Biophys. Acta 1780*, 948–959.
54. Reshetnyak, Y. K., Andreev, O. A., Segala, M., Markin, V. S., and Engelman, D. M. (2008) Energetics of peptide (pHLIP) binding to and folding across a lipid bilayer membrane. *Proc. Natl. Acad. Sci. U.S.A. 105*, 15340–15345.
55. Wi, S., and Kim, C. (2008) Pore structure, thinning effect, and lateral diffusive dynamics of oriented lipid membranes interacting with antimicrobial peptide protegrin-1: ^{31}P and ^{2}H solid-state NMR study. *J. Phys. Chem. B 112*, 11402–11414.
56. Hallock, K. J., Lee, D.-K., and Ramamoorthy, A. (2003) MSI-78, an analogue of the magainin antimicrobial peptides, disrupts lipid bilayer structure via positive curvature strain. *Biophys. J. 84*, 3052–3060.
57. Morein, S., Andersson, A., Rilfors, L., and Lindblom, G. (1996) Wild-type *Escherichia coli* cells regulate the membrane lipid composition in a "window" between gel and non-lamellar structures. *J. Biol. Chem. 271*, 6801–6809.
58. Nguyen, K. T., Le Clair, S. V., Ye, S., and Chen, Z. (2009) Orientation Determination of Protein Helical Secondary Structures Using Linear and Nonlinear Vibrational Spectroscopy. *J. Phys. Chem. B 113*, 12169–12180.

59. Lee, K. H., Hong, S. Y., Oh, J. E., Kwon, M. Y., Yoon, J. H., Lee, J. H., Lee, B. L., and Moon, H. M. (1998) Identification and characterization of the antimicrobial peptide corresponding to C-terminal β-sheet domain of tenecin 1, an antibacterial protein of larvae of *Tenebrio molitor*. *Biochem. J. 334*, 99–105.
60. Andrushchenko, V. V., Aarabi, M. H., Nguyen, L. T., Prenner, E. J., and Vogel, H. J. (2008) Thermodynamics of the interactions of tryptophan-rich cathelicidin antimicrobial peptides with model and natural membranes. *Biochim. Biophys. Acta 1778*, 1004–1014.
61. Park, S.-C., Kim, M.-H., Hossain, M. A., Shin, S. Y., Kim, Y., Stella, L., Wade, J. D., Park, Y., and Hahm, K.-S. (2008) Amphipathic α-helical peptide, HP (2−20), and its analogues derived from *Helicobacter pylori*: Pore formation mechanism in various lipid compositions. *Biochim. Biophys. Acta 1778*, 229–241.
62. Rodríguez, A., Villegas, E., Satake, H., Possani, L. D., and Corzo, G. (2010) Amino acid substitutions in an α-helical antimicrobial arachnid peptide affect its chemical properties and biological activity towards pathogenic bacteria but improves its therapeutic index. *Amino Acids* (in press).
63. Pouny, Y., and Shai, Y. (1992) Interaction of D-amino-acid incorporated analogs of paradoxin with membranes. *Biochemistry 31*, 9482–9490.
64. Cheng, J. T. J., Hale, J. D., Elliot, M., Hancock, R. E. W., and Straus, S. K. (2009) Effect of Membrane Composition on Antimicrobial Peptides Aurein 2.2 and 2.3 From Australian Southern Bell Frogs. *Biophys. J. 96*, 552–565. Epand, R. M., and Vogel, H. J. (1999) Diversity of antimicrobial peptides and their mechanisms of action. *Biochim. Biophys. Acta 1462*, 11–28.
65. Oren, Z., and Shai, Y. (2000) Cyclization of a cytolytic amphipathic α-helical peptide and its diastereomer: Effect on structure, interaction with model membranes, and biological function. *Biochemistry 39*, 6103–6114.
66. Henriques, S. T., and Castanho, M. A. R. B. (2004) Consequences of nonlytic membrane perturbation to the translocation of the cell penetrating peptide pep-1 in lipidic vesicles. *Biochemistry 43*, 9716–9724.
67. Lequin, O., Ladram, A., Chabbert, L., Bruston, F., Convert, O., Vanhoye, D., Chassaing, G., Nicolas, P., and Amiche, M. (2006) Dermaseptin S9, an α-helical antimicrobial peptide with a hydrophobic core and cationic termini. *Biochemistry 45*, 468–480.
68. Ramamoorthy, A., Thennarasu, S., Lee, D.-K., Tan, A., and Maloy, L. (2006) Solid-state NMR investigation of the membrane-disrupting mechanism of antimicrobial peptides MSI-78 and MSI-594 derived from magainin 2 and melittin. *Biophys. J. 91*, 206–216.
69. Rozek, A., Friedrich, C. L., and Hancock, R. E. W. (2000) Structure of the bovine antimicrobial peptide indolicidin bound to dodecylphosphocholine and sodium dodecyl sulfate micelles. *Biochemistry 39*, 15765–15774.
70. Schibli, D. J., Nguyen, L. T., Kernaghan, S. D., Rekdal, Ø., and Vogel, H. J. (2006) Structure-function analysis of tritrpticin analogs: Potential relationships between antimicrobial activities, model membrane interactions, and their micelle-bound NMR structures. *Biophys. J. 91*, 4413–4426.
71. Bechinger, B. (1996) Towards membrane protein design: pH-sensitive topology of histidine-containing polypeptides. *J. Mol. Biol. 263*, 768–775.